

# MCRB-based Performance Analysis of 6G Localization under Hardware Impairments

Hui Chen\*, Sina Rezaei Aghdam\*, Musa Furkan Keskin\*, Yibo Wu\*†, Simon Lindberg†,  
Andreas Wolfgang†, Ulf Gustavsson†, Thomas Eriksson\*, Henk Wymeersch\*

\*Chalmers University of Technology, Sweden, †Qamcom Research & Technology, Sweden,  
†Ericsson Research, Sweden  
e-mail: hui.chen@chalmers.se

**Abstract**—Location information is expected to be the key to meeting the needs of communication and context-aware services in 6G systems. User localization is achieved based on delay and/or angle estimation using uplink or downlink pilot signals. However, hardware impairments (HWIs) distort the signals at both the transmitter and receiver sides and thus affect the localization performance. While this impact can be ignored at lower frequencies where HWIs are less severe, modeling and analysis efforts are needed for 6G to evaluate the localization degradation due to HWIs. In this work, we model various types of impairments and conduct a misspecified Cramér-Rao bound analysis to evaluate the HWI-induced performance loss. Simulation results with different types of HWIs show that each HWI leads to a different level of degradation in angle and delay estimation performance.

**Index Terms**—Localization, 5G/6G, hardware impairment, CRB, MCRB.

## I. INTRODUCTION

Localization will be an indispensable part of future communication systems, both to improve spatial efficiency and optimize resource allocation [1], but also to support high-accuracy context-aware applications such as the tactile internet, augmented reality, and smart cities [2], [3]. By taking advantage of a large array dimension and wide bandwidth of high-frequency (e.g., mmWave and sub-THz) communication systems, high angular and delay resolution, and hence accurate position estimation can be achieved [4]. Most localization algorithms rely on accurate models of the received signals as a function of the channel parameters (angles, delays, Dopplers) of the propagation environment. The presence of hardware impairments (HWIs) such as phase noise (PN), carrier frequency offset (CFO), mutual coupling (MC), power amplifier nonlinearity (PAN), in-phase and quadrature imbalance (IQI), distort the pilot signals. As a result, when algorithms derived from a mismatched model (i.e., without or with limited information about the HWIs), the localization performance is unavoidably affected.

There has been extensive research on the effect of HWIs in communication systems in terms of spectral efficiency analysis [5], beamforming optimization [6], and channel estimation [7], [8]. The research on localization and sensing considering HWIs is also catching up. The effect of PN on automotive radar [9]–[11], mutual coupling on DOA estimation [12], IQI on mmWave localization [13], and PAN on

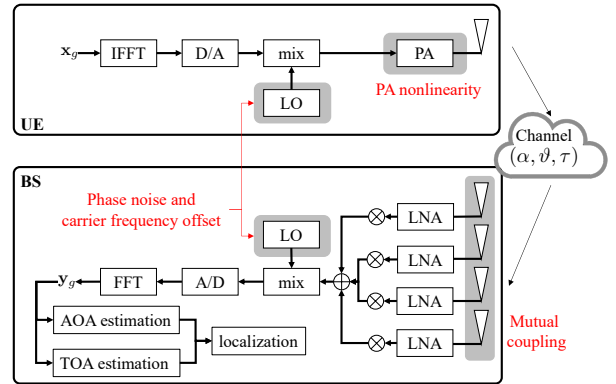


Fig. 1. Block diagram of considered hardware impairments (marked in gray) at transmitter and receiver. When the localization algorithm does not have perfect knowledge of the generative model, it operates under model mismatch.

joint radar-communication (JRC) systems [14] are discussed. In [15], the impairments are jointly modeled using a HWI factor. Nevertheless, this factor is not able to capture the contribution of each individual HWI. Hence, critical questions, such as how much error will be caused by a mismatched model, and how much HWI we can tolerate for 5G/6G localization, remain unanswered.

In this work, we consider an orthogonal frequency-division multiplexing (OFDM)-based localization system with HWIs. The corresponding localization algorithm may or may not have knowledge about these HWIs, where in the latter case the localization algorithm operates under model mismatch, as it does not know the PAN and the residual impairments of PN, CFO, and MC. We use the Cramér-Rao bound (CRB) to predict the performance in angle, delay, and position estimation under the different models, and employ the misspecified Cramér-Rao bound (MCRB) [16]–[18] to quantify the estimation performance loss due to model mismatch. The results show that different types of impairments affect angle and delay estimation in different ways.

## II. SYSTEM MODEL

In this section, we start with the HWI-free model and then describe the HWI model, as shown in Fig. 1. We consider a simplified uplink scenario with a line-of-sight (LOS) channel between a base station (BS) equipped with an  $N$ -antenna

uniform linear array (ULA) and a synchronized single-antenna user equipment (UE), both with a single radio-frequency chain (RFC). The assumptions of single-antenna UE, perfect synchronization, and pure LOS may not be realistic in practice, but are an initial step to analyze and understand HWIs. We set the center of the BS array as the origin of the global coordinate system. The relation between the angle-of-arrival (AOA)  $\vartheta$ , the delay  $\tau$ , and the UE position  $\mathbf{p}$  can be expressed as  $\mathbf{p} = \tau c [\cos(\vartheta), \sin(\vartheta)]^\top$ , where  $c$  is the speed of light.

### A. Hardware Impairment-free Model

Considering the transmitted OFDM symbol at  $g$ -th transmission ( $1 \leq g \leq \mathcal{G}$ ) and  $k$ -th subcarrier ( $1 \leq k \leq K$ ),  $x_{g,k}$ , its observation at the BS can be formulated as

$$y_{g,k} = \mathbf{w}_g^\top \mathbf{h}_k x_{g,k} + n_{g,k}, \quad (1)$$

where  $\mathbf{w}_g \in \mathbb{C}^N$  is the combiner at the BS for the  $g$ -th transmission;  $\mathbf{h}_k = \alpha D_k \mathbf{a}(\vartheta)$  is the channel vector at the  $k$ th subcarrier with a complex gain (amplitude  $\rho$  and phase  $\xi$ ) as  $\alpha = \rho e^{-j\xi} = \lambda e^{-j\xi}/(4\pi c\tau)$ , an receiver steering vector  $\mathbf{a}(\vartheta) = [1, e^{j\pi \sin(\vartheta)}, \dots, e^{j(N-1)\pi \sin(\vartheta)}]^\top$ , and a delay component  $D_k = e^{-j2\pi k \Delta_f \tau}$  ( $\Delta_f$  is the subcarrier spacing). We assume  $\mathbf{h}_k$  remains the same during  $\mathcal{G}$  transmissions (within the coherence time). Finally,  $n_{g,k} \in \mathcal{CN}(0, \sigma_n^2)$  is the noise following a complex normal distribution, with  $\sigma_n^2 = N_0 W$ , where  $N_0$  is the noise power spectral density (PSD) and  $W = K \Delta_f$  is the total bandwidth. The average transmission power  $P = \mathbb{E}\{|x_{g,k}|^2\}/R$ , where  $R$  is the load impedance. By concatenating all the received symbols into a column, we obtain the received symbol block  $\mathbf{y} \in \mathbb{R}^{GK}$  as  $\mathbf{y} = [\mathbf{y}_1^\top, \dots, \mathbf{y}_g^\top, \dots, \mathbf{y}_G^\top]^\top$ , where  $\mathbf{y}_g = [y_{g,1}, \dots, y_{g,K}]^\top$  can be expressed as

$$\mathbf{y}_g = \alpha \mathbf{w}_g^\top \mathbf{a}(\vartheta) \mathbf{d}(\tau) \odot \mathbf{x}_g + \mathbf{n}_g \quad (2)$$

in which  $\mathbf{d}(\tau) = [D_1, \dots, D_K]^\top$ ,  $\mathbf{x}_g = [x_{g,1}, \dots, x_{g,K}]^\top$ ,  $\mathbf{n}_g = [n_{g,1}, \dots, n_{g,K}]^\top$  and  $\odot$  denotes the Hadamard product.

### B. Hardware Impairments

The considered HWIs are highlighted in gray in Fig. 1 [19]. We select residual PN, residual CFO, residual MC, and PAN. The IQI and imperfections of analog to digital converter (ADC), digital to analog converter (DAC), low-noise amplifier (LNA) and mixer are left for future work. By focusing on residual PN, CFO, and MC, our analysis can impose requirements on the corresponding PN, CFO, and MC estimation accuracy.

1) *Phase Noise and Carrier Frequency Offset*: Imperfect local oscillators (LOs) in the up-conversion and down-conversion processes add PN to the carrier wave phase. In addition, when the down-converting LO in the receiver does not perfectly synchronize with the received signal's carrier [20], CFO occurs. Generally, both PN and CFO are tackled by the receiver [21], so we only consider the residual PN and residual CFO at the receiver. With PN and CFO, the observation,  $y_{g,k}$ , is modified as [22]

$$y_{g,k} \rightarrow \mathbf{f}_k^\top \mathbf{E}_g \mathbf{\Xi}_g \mathbf{F}^\top \mathbf{y}_g, \quad (3)$$

where  $\mathbf{y}_g$  is without PN or CFO (i.e., from (1)),  $\mathbf{F} = [\mathbf{f}_1, \mathbf{f}_2, \dots, \mathbf{f}_K]$  is the FFT matrix,

$$\mathbf{\Xi}_g = \text{diag}([e^{j\omega_{g,1}}, \dots, e^{j\omega_{g,K}}]) \quad (4)$$

is the residual<sup>1</sup> phase noise matrix with  $\omega_{g,k} \sim \mathcal{N}(0, \sigma_{\text{PN}}^2)$ , and  $\mathbf{E}_g$  accounts for the CFO. In (3), the vector  $\mathbf{y}_g$  is converted to the time domain by  $\mathbf{F}^\top \mathbf{y}_g$ , where the successive phase noise samples, as well as the CFO are applied. Finally,  $\mathbf{f}_k^\top$  extracts the  $k$ -th subcarrier after applying an FFT to  $\mathbf{E}_g \mathbf{\Xi}_g \mathbf{F}^\top \mathbf{y}_g$ . The CFO matrix  $\mathbf{E}_g$  considers both inter-OFDM symbol phase changes as well as inter-carrier interference [22], [25]:

$$\mathbf{E}_g = e^{j\frac{2\pi \epsilon g K_{\text{tot}}}{K}} \text{diag}([1, e^{j\frac{2\pi \epsilon}{K}}, \dots, e^{j\frac{2\pi(K-1)\epsilon}{K}}]), \quad (5)$$

where  $K_{\text{tot}} = K + K_{\text{cp}}$ , in which  $K_{\text{cp}}$  is the length of the cyclic prefix, and  $\epsilon$  is the normalized residual CFO with  $\epsilon \sim \mathcal{N}(0, \sigma_{\text{CFO}}^2)$ .

2) *Mutual Coupling*: MC refers to the electromagnetic interaction between the antenna elements in an array [12]. Similar to PN and CFO modeling, we consider residual MC, which remains after a calibration procedure. For a ULA, we introduce the banded MC matrix  $\mathbf{C} \in \mathbb{C}^{N \times N} = \tilde{\mathbf{C}} + \Delta_{\text{MC}}$  at the Rx. Here,  $\tilde{\mathbf{C}} = \text{Toeplitz}([1, c_1, \dots, c_n, 0, \dots, 0])$  is the MC matrix with  $c_n$  as the MC coefficient, and  $\Delta_{\text{MC}}$  represents the uncalibrated MC matrix that is modeled as random (residual MC matrix) with each element  $\Delta_{i,j} \sim \mathcal{N}(0, \sigma_{\text{MC}}^2)$ . The MC leads to the substitution [12]

$$\mathbf{h}_k \rightarrow \mathbf{C} \mathbf{h}_k. \quad (6)$$

3) *Power Amplifier Nonlinearity*: For the PA nonlinearity, we consider a  $Q$ -th order memoryless polynomial nonlinear model with a clipping point  $x_{\text{clip}} \in \mathbb{R}$  as [19]

$$h_{\text{PA}}(\check{x}) = \begin{cases} \sum_{q=0}^Q \beta_q \check{x} |\check{x}|^q & |\check{x}| \leq x_{\text{clip}}, \\ \sum_{q=0}^Q \beta_q \frac{\check{x}}{|\check{x}|} |x_{\text{clip}}|^q & |\check{x}| > x_{\text{clip}}, \end{cases} \quad (7)$$

where  $\check{x}$  denotes the transmitted signals in time domain and  $\beta_0, \dots, \beta_Q$  are complex-valued parameters. Note that the PA affects the time domain signals and we assume no digital pre-distortion is implemented. We also use non-oversampled signals as the input of the PA for tractable localization performance analysis.

### C. Hardware Impaired Model

Considering the HWIs of PN, CFO, MC, and PA nonlinearity and substituting (3), (6), and (7) into (2), the observation can be rewritten in the frequency domain as

$$\begin{aligned} \mathbf{y}_g &= \alpha \mathbf{F} \mathbf{E}_g \mathbf{\Xi}_g \mathbf{F}^\top (\mathbf{w}_g^\top \mathbf{C} \mathbf{a}(\vartheta)) \mathbf{d}(\tau) \\ &\quad \odot (\mathbf{F}^\top \mathbf{h}_{\text{PA}}(\mathbf{F}^\top \mathbf{x}_g)) + \mathbf{n}_g \\ &= \alpha \bar{\mathbf{\eta}}_g(\mathbf{p}) + \mathbf{n}_g = \bar{\mathbf{\mu}}_g(\alpha, \mathbf{p}) + \mathbf{n}_g, \end{aligned} \quad (8)$$

where  $\mathbf{h}_{\text{PA}}(\cdot)$  overloads the notation for the PA, and operates point-wise on each of the elements in the time-domain sequence. The FFT and IFFT matrices switch between time and

<sup>1</sup>Since  $\omega_{g,k}$  represents residual PN that remains after PN mitigation processing (e.g., [23], [24]), it is assumed to be independent across time.

frequency domain representations in order to apply the PN, CFO and PA in the correct (time) domain, while providing a frequency domain representation. We use  $\bar{\mu}_g(\alpha, \mathbf{p})$  to denote the noise-free observation. Note that the PA model in (7) does not consider the out-of-band emissions, but only the in-band distortion.

Finally, we consider a model without the PAN and the residual noise of PN, CFO, and MC:

$$\begin{aligned} \mathbf{y}_g &= \alpha \mathbf{w}_g^\top \tilde{\mathbf{C}} \mathbf{a}(\vartheta) \mathbf{d}(\tau) \odot \mathbf{x}_g + \mathbf{n}_g \\ &= \alpha \boldsymbol{\eta}_g(\mathbf{p}) + \mathbf{n}_g = \boldsymbol{\mu}_g(\alpha, \mathbf{p}) + \mathbf{n}_g, \end{aligned} \quad (9)$$

where  $\boldsymbol{\mu}_g(\alpha, \mathbf{p})$  is the noise-free version of the observation.

#### D. Summary of the Models

To summarize, we have defined three types of signal models as follows.

- **M0:** The model defined in (1) without considering the HWI.
- **M1:** The model that considers knowledge of the various HWIs defined in (8).
- **M2:** With the practical assumption that not all the HWIs information is available, we use the model defined in (9).

In the rest of the work, M0 will not be discussed, and the models M1 and M2 will be used for CRB analysis, as well as for localization performance evaluation.

### III. LOCALIZATION ALGORITHM

The maximum likelihood estimation (MLE) is employed when the observation  $\mathbf{y}$  is generated from the same model used by the algorithm. On the other hand, the mismatched maximum likelihood estimation (MMLE) is used when the observation  $\mathbf{y}$  is generated from a different model than what is used by the algorithm. In the latter case, we will denote the generative model by *true model (TM)*, while the model used by the estimator is called the *mismatched model (MM)*.

#### A. MLE

If  $\mathbf{y} \sim f_{\text{TM}}(\mathbf{y}|\alpha, \mathbf{p})$ , the MLE of the UE position and channel gain is

$$[\hat{\mathbf{p}}_{\text{MLE}}, \hat{\alpha}_{\text{MLE}}] = \arg \max_{\mathbf{p}, \alpha} \ln f_{\text{TM}}(\mathbf{y}|\alpha, \mathbf{p}), \quad (10)$$

where  $\ln f_{\text{TM}}(\mathbf{y}|\alpha, \mathbf{p})$  is the log-likelihood of the TM. Since  $\alpha$  appears linearly in the noise-free observation, we can use a plug-in estimate, and solve for the position by a coarse grid search to find an initial estimate  $\mathbf{p}_0$ , followed by a backtracking line search [26]. For instance, when  $\text{TM} = \mathbf{M1}$ ,

$$\hat{\mathbf{p}}_{\text{MLE}} = \arg \min_{\mathbf{p}} \left\| \mathbf{y} - \frac{\bar{\boldsymbol{\eta}}(\mathbf{p})^\top \mathbf{y}}{\|\bar{\boldsymbol{\eta}}(\mathbf{p})\|^2} \bar{\boldsymbol{\eta}}(\mathbf{p}) \right\|^2. \quad (11)$$

#### B. MMLE

If  $\mathbf{y} \sim f_{\text{TM}}(\mathbf{y}|\alpha, \mathbf{p})$ , but the estimator uses  $f_{\text{MM}}(\mathbf{y}|\alpha, \mathbf{p}) \neq f_{\text{TM}}(\mathbf{y}|\alpha, \mathbf{p})$ , the MMLE is given by

$$[\hat{\mathbf{p}}_{\text{MMLE}}, \hat{\alpha}_{\text{MMLE}}] = \arg \max_{\mathbf{p}, \alpha} \ln f_{\text{MM}}(\mathbf{y}|\alpha, \mathbf{p}), \quad (12)$$

For instance, when  $\text{MM} = \mathbf{M2}$  and  $\text{TM} \neq \mathbf{M2}$ ,

$$\hat{\mathbf{p}}_{\text{MMLE}} = \arg \min_{\mathbf{p}} \left\| \mathbf{y} - \frac{\boldsymbol{\eta}(\mathbf{p})^\top \mathbf{y}}{\|\boldsymbol{\eta}(\mathbf{p})\|^2} \boldsymbol{\eta}(\mathbf{p}) \right\|^2. \quad (13)$$

### IV. LOWER BOUNDS ANALYSIS

In the next, we derive the CRB for  $\text{M2}^2$ , as well as the MCRB for the mismatched estimator in (13) with  $\text{TM} = \mathbf{M1}$  and  $\text{MM} = \mathbf{M2}$ .

#### A. CRB Analysis

We define a channel parameter vector as  $\boldsymbol{\theta} = [\vartheta, \tau, \rho, \xi]^\top$  and a state vector  $\mathbf{s} = [p_x, p_y, \rho, \xi]^\top$ . Given the signal model in (9) and  $\mathbf{y} \sim f_{\text{MM}}(\mathbf{y}|\alpha, \mathbf{p})$ , the CRB of the MM can be obtained as [27]

$$\text{CRB} \triangleq [\mathbf{I}(\mathbf{s})]^{-1} = [\mathbf{J}_S^\top \mathbf{I}(\boldsymbol{\theta}) \mathbf{J}_S]^{-1}, \quad (14)$$

where

$$\mathbf{I}(\boldsymbol{\theta}) = \frac{2}{\sigma_n^2} \sum_{g=1}^G \sum_{k=1}^K \text{Re} \left\{ \left( \frac{\partial \mu_{g,k}}{\partial \boldsymbol{\theta}} \right)^\top \left( \frac{\partial \mu_{g,k}}{\partial \boldsymbol{\theta}} \right) \right\}, \quad (15)$$

$$\mathbf{J}_S \triangleq \frac{\partial \boldsymbol{\theta}}{\partial \mathbf{s}} = \begin{bmatrix} \frac{\partial \vartheta}{\partial p_x} & \frac{\partial \vartheta}{\partial p_y} & 0 & 0 \\ \frac{\partial \tau}{\partial p_x} & \frac{\partial \tau}{\partial p_y} & 0 & 0 \\ 0 & 0 & 1 & 0 \\ 0 & 0 & 0 & 1 \end{bmatrix}. \quad (16)$$

Here,  $\mathbf{I}(\boldsymbol{\theta})$ ,  $\mathbf{I}(\mathbf{s})$  are the Fisher information matrices (FIMs) of the channel parameter vector and UE state vector,  $\text{Re}\{\cdot\}$  is getting the real part of a complex number, and  $\mathbf{J}_S$  is the Jacobian matrix using a denominator-layout notation with  $\partial \boldsymbol{\theta} / \partial \mathbf{p} = 1/(c\tau) [-\sin(\vartheta) \cos(\vartheta)]^\top$  and  $\partial \tau / \partial \mathbf{p} = \mathbf{p}/(c\tau)$ . Based on the FIM, we further define the angle error bound (AEB), delay error bound (DEB) and position error bound (PEB) as

$$\text{AEB} = \sqrt{([\mathbf{I}(\boldsymbol{\theta})^{-1}]_{1,1})}, \quad (17)$$

$$\text{DEB} = \sqrt{([\mathbf{I}(\boldsymbol{\theta})^{-1}]_{2,2})}, \quad (18)$$

$$\text{PEB} = \sqrt{\text{tr}([\text{CRB}]_{1:2,1:2})}, \quad (19)$$

where  $\text{tr}(\cdot)$  returns the trace of a matrix, and  $[\cdot]_{i,j}$  is getting the element in the  $i$ th row,  $j$ th column of a matrix. The bounds from (17)–(19) will be used to evaluate the localization performance.

#### B. Misspecified CRB

The model is said to be mismatched or misspecified when  $\mathbf{y} \sim f_{\text{TM}}(\mathbf{y}|\alpha, \mathbf{p})$ , while the estimation is based on the assumption that  $\mathbf{y} \sim f_{\text{MM}}(\mathbf{y}|\alpha, \mathbf{p})$ , where  $f_{\text{TM}}(\mathbf{y}|\alpha, \mathbf{p}) \neq f_{\text{MM}}(\mathbf{y}|\alpha, \mathbf{p})$ . Due to the one-to-one mapping between  $\mathbf{s}$  and  $\boldsymbol{\theta}$ , we can also write  $f_{\text{TM}}(\mathbf{y}|\boldsymbol{\theta})$  and  $f_{\text{MM}}(\mathbf{y}|\boldsymbol{\theta})$ . The lower bound (LB) of using a mismatched estimator can be obtained as [18]

$$\begin{aligned} \text{LB}(\bar{\boldsymbol{\theta}}, \boldsymbol{\theta}_0) &= \underbrace{\mathbf{A}_{\boldsymbol{\theta}_0}^{-1} \mathbf{B}_{\boldsymbol{\theta}_0} \mathbf{A}_{\boldsymbol{\theta}_0}^{-1}}_{=\text{MCRB}(\boldsymbol{\theta}_0)} + \underbrace{(\bar{\boldsymbol{\theta}} - \boldsymbol{\theta}_0)(\bar{\boldsymbol{\theta}} - \boldsymbol{\theta}_0)^\top}_{=\text{Bias}(\boldsymbol{\theta}_0)}, \end{aligned} \quad (20)$$

<sup>2</sup>The CRB of M1 can be obtained similarly, which will not be detailed in this work.

where  $\bar{\theta}$  is the true channel parameter vector,  $\theta_0$  is the pseudo-true parameter vector (which will be introduced soon), and  $\mathbf{A}_{\theta_0}, \mathbf{B}_{\theta_0}$  are two possible generalizations of the FIMs. The LB is a bound in the sense that (typo ‘ $(\text{LB}(\bar{\theta}, \theta_0))^{-1}$ , is corrected as ‘ $\text{LB}(\bar{\theta}, \theta_0)$ ’)

$$\mathbb{E}\{(\hat{\theta}_{\text{MMLE}} - \bar{\theta})(\hat{\theta}_{\text{MMLE}} - \bar{\theta})^\top\} \succeq \text{LB}(\bar{\theta}, \theta_0), \quad (21)$$

where the expectation is with respect to  $f_{\text{TM}}(\mathbf{y}|\theta)$ . What remains is the formal definition and computation of the pseudo-true parameter  $\theta_0$  and  $\mathbf{A}_{\theta_0}, \mathbf{B}_{\theta_0}$ .

1) *Pseudo-true Parameter*: Assume the probability density function (PDF) of the TM, where the observation data come from, is  $f_{\text{TM}}(\mathbf{y}|\bar{\theta})$ , where  $\mathbf{y}$  is the received signals and  $\bar{\theta} \in \mathbb{R}^4$  (4 unknowns for this 2D case) is the vector containing all the channel parameters. Similarly, the PDF of the MM for the received signal  $\mathbf{y}$  can be noted as  $f_{\text{MM}}(\mathbf{y}, \theta)$ . The pseudo-true parameter vector is defined as the point that minimizes the Kullback-Leibler divergence between  $f_{\text{TM}}(\mathbf{y}|\bar{\theta})$  and  $f_{\text{MM}}(\mathbf{y}|\theta)$  as

$$\theta_0 = \arg \min_{\theta} D_{\text{KL}}(f_{\text{TM}}(\mathbf{y}|\bar{\theta}) \| f_{\text{MM}}(\mathbf{y}|\theta)). \quad (22)$$

We define  $\epsilon(\theta) \triangleq \bar{\mu}(\bar{\theta}) - \mu(\theta)$ , and the pseudo-true parameter can be obtained as (details can be found in Appendix A)

$$\theta_0 = \arg \min_{\theta} \|\epsilon(\theta)\|^2 = \arg \min_{\theta} \|\bar{\mu}(\bar{\theta}) - \mu(\theta)\|^2. \quad (23)$$

Hence,  $\theta_0$  can be found by solving (13) with the observation  $\mathbf{y} = \bar{\mu}(\bar{\theta})$ , which can be accomplished using the same algorithm in Sec. III, initialized with the true value  $\bar{\theta}$ .

2) *MCRB Component Matrices*: The matrices  $\mathbf{A}_{\theta_0}$  and  $\mathbf{B}_{\theta_0}$  can be obtained based on the pseudo-true parameter vector  $\theta_0$  as

$$\begin{aligned} [\mathbf{A}_{\theta_0}]_{i,j} &= \int \frac{\partial^2 \ln f_{\text{MM}}(\mathbf{y}|\theta)}{\partial \theta_i \partial \theta_j} f_{\text{TM}}(\mathbf{y}|\bar{\theta}) d\mathbf{y} \Big|_{\theta=\theta_0} \\ &= -\frac{1}{\sigma_n^2} \sum_{g,k} \int \frac{\partial^2 |y_{g,k} - \mu_{g,k}(\theta)|^2}{\partial \theta_i \partial \theta_j} f_{\text{TM}}(y_{g,k}|\bar{\theta}) d y_{g,k} \Big|_{\theta=\theta_0} \\ &= \frac{2}{\sigma_n^2} \text{Re} \left[ \frac{\partial^2 \mu(\theta)}{\partial \theta_i \partial \theta_j} \epsilon(\theta) - \frac{\partial \mu(\theta)}{\partial \theta_j} \left( \frac{\partial \mu(\theta)}{\partial \theta_i} \right)^H \right] \Big|_{\theta=\theta_0} \end{aligned} \quad (24)$$

and

$$\begin{aligned} [\mathbf{B}_{\theta_0}]_{i,j} &= \int \frac{\partial \ln f_{\text{MM}}(\mathbf{y}|\theta)}{\partial \theta_i} \frac{\partial \ln f_{\text{MM}}(\mathbf{y}|\theta)}{\partial \theta_j} f_{\text{TM}}(\mathbf{y}|\bar{\theta}) d\mathbf{y} \Big|_{\theta=\theta_0} \\ &= \frac{1}{\sigma_n^4} \int \sum_{g,k} \sum_{g',k'} \frac{\partial |y_{g,k} - \mu_{g,k}(\theta)|^2}{\partial \theta_i} \\ &\quad \times \frac{\partial |y_{g',k'} - \mu_{g',k'}(\theta)|^2}{\partial \theta_j} f_{\text{TM}}(\mathbf{y}|\bar{\theta}) d\mathbf{y} \\ &= \frac{4}{\sigma_n^4} \text{Re} \left[ \frac{\partial^2 \mu(\theta)}{\partial \theta_i} \epsilon(\theta) \right] \text{Re} \left[ \frac{\partial^2 \mu(\theta)}{\partial \theta_j} \epsilon(\theta) \right] \\ &\quad + \frac{2}{\sigma_n^2} \text{Re} \left[ \frac{\partial \mu(\theta)}{\partial \theta_j} \left( \frac{\partial \mu(\theta)}{\partial \theta_i} \right)^H \right] \Big|_{\theta=\theta_0}. \end{aligned} \quad (25)$$

where the calculation of each element inside the matrices  $\mathbf{A}_{\theta_0}$  and  $\mathbf{B}_{\theta_0}$  can be found in Appendix B.

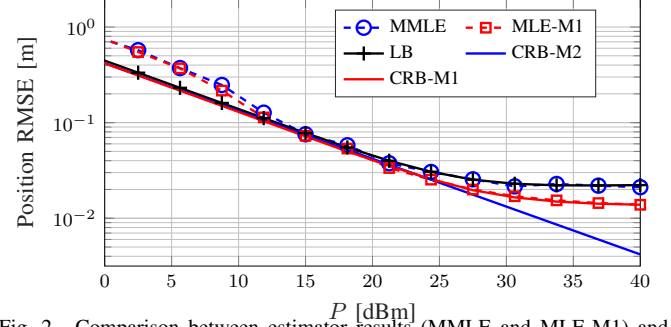


Fig. 2. Comparison between estimator results (MMLE and MLE-M1) and different lower bounds. Due to the HWIs, the performance saturates when the transmission power exceeds 30 dBm. However, with the knowledge of the impairments, the bound (red curve with square markers) could be lower than the LB (blue curve with circle markers).

## V. NUMERICAL RESULTS

### A. Default Parameters

We consider a 2D uplink scenario with a single-antenna UE and a BS with a 20-element ULA. The pilot signal  $x_{g,k}$  is chosen with a constant average energy  $|x_{g,k}|^2 = PR$  and random phase. The simulation parameters<sup>3</sup> can be found in Table I.

TABLE I  
DEFAULT SIMULATION PARAMETERS

Parameters	True Model	Mismatched Model
BS Antennas	$N = 10$	
UE Antennas	1	
RFC at BS/UE	1	
Carrier Frequency	$f_c = 140$ GHz	
Bandwidth	$W = 1$ GHz	
Transmissions	$G = 10$	
Subcarriers	$K = 100$	
Length of the CP	$K_{\text{cp}} = 7$	
Load Impedance	$R = 50 \Omega$	
Noise PSD	$N_0 = -173.855$ dBm/Hz	
Noise Figure	10 dBm	
PN (residue)	$\sigma_{\text{PN}} = 10^\circ$	$\sigma_{\text{PN}} = 0^\circ$
CFO (residue)	$\sigma_{\text{CFO}} = 0.01$ (0.71 ppm)	$\sigma_{\text{CFO}} = 0$
MC (matrix)	$c_1 = 0.6 + 0.5j, c_2 = 0.4054 - 0.128j$	
MC (residue)	$\sigma_{\text{MC}} = 0.02$	$\sigma_{\text{MC}} = 0$
PA Parameters	$\beta_0 = 0.9798 + 0.0286j, \beta_1 = 0.0122 - 0.0043j$	$\beta_2 = -0.0007 + 0.0001j$
PA Clipping Voltage	$x_{\text{clip}} = 25V$	

### B. Estimation Results vs. Bounds

We first evaluate the position estimation performance of the two estimators (MLE (11) and MMLE (13), where observations come from the hardware-impaired model M1). The simulation results are compared with three different lower bounds, namely, LB (the lower bound of using the M2 to process the data from the M1), CRB-M1, and CRB-M2. Note that the average transmission power  $P$  is calculated without considering the nonlinearity of the power amplifier (calculated before the PA). Fig. 2 shows the positioning errors obtained

<sup>3</sup>The PA parameters are estimated from the measurements of the RF WebLab, which can be remotely accessed at [www.dpcompetition.com](http://www.dpcompetition.com).

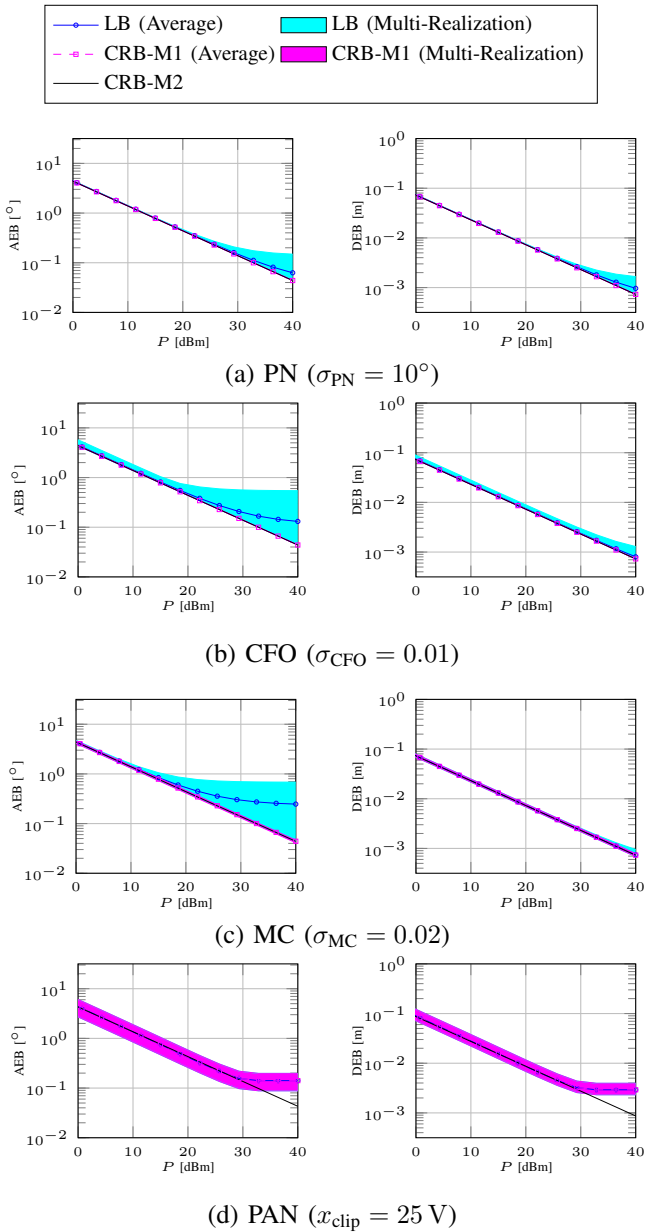


Fig. 3. AEB (left) and DEB (right) for multiple realizations: (a) Phase noise, (b) Carrier frequency offset, (c) Mutual coupling, (d) Power amplifier nonlinearity.

by the estimators, along with the corresponding theoretical bounds, with respect to  $P$ . From the figure, we can see that at low transmit powers, the LB and CRBs coincide, implying that the HWIs are not the main source of error. At higher transmit powers (after 20 dBm), LB deviates from the CRBs and the positioning performance is thus more severely affected by HWIs. The MMLE closely follows the LB, indicating the validity of the LB. In terms of CRB-M1, we observe the bound converges to a certain value after 30 dBm, due to the PAN, while the CRB-M2 keeps a fixed downward trend.

#### C. The Effect of Individual Impairments

To gain a deeper understanding, we study the impact of HWIs on angle and delay estimation, considering different

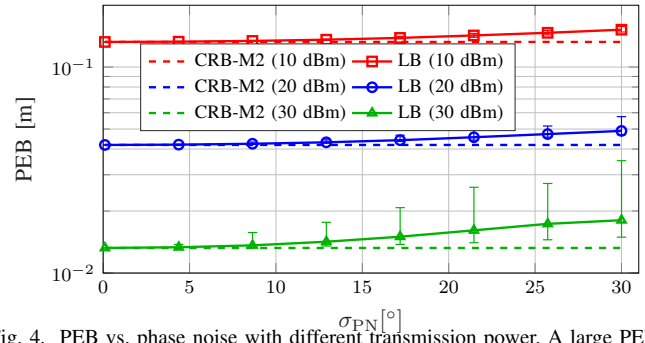


Fig. 4. PEB vs. phase noise with different transmission power. A large PEB variance is observed in the scenarios with high SNR or large PN level.

HWIs separately. The results are shown in Fig. 3 for (a) PN, (b) CFO, (c) MC, and (d) PAN. Multiple realizations (multiple hardware realizations with a fixed pilot signal for (a)-(c) and multiple pilot signal realizations for (d)) are performed for each type of the HWI. We can see that different types of the HWIs affect angle and delay estimation differently. The PN and PAN affect both angle and delay estimation, however, the effect of PAN is mainly caused by the distortion of the pilot signals, whereas the effect of PN depends on the residual noise level  $\sigma_{\text{PN}}$ . The CFO and MC have a more significant effect on angle estimation compared to delay estimation since the CFO affects the phase changes across beams and the MC distorts the steering vector. In addition, within reasonable levels of hardware impairments, the CRBs with perfect knowledge of the impairments (CRB-M1) are close to the CRBs of the MM (CRB-M2).

In Fig. 4, we evaluate the localization performance (which in turn depends on the AEB (in terms of degree) and DEB (in terms of meter) shown in Fig. 3) as a function of the standard deviation of PN  $\sigma_{\text{PN}}$  (similar patterns can be seen for CFO and MC) for various values of average transmission power using 100 realizations of PN. The impairments produce a larger perturbation in the high SNR scenario. As for low SNR, the noise level is high enough and the impairments, under a certain level, will not degrade the PEB too much.

## VI. CONCLUSION

HWIs present a crucial roadblock to achieving high performance in radio-based localization. We modeled different types of HWIs and utilize the MCRB to evaluate the error caused by model-mismatch. The effects of residual PN, residual CFO, residual MC and PAN on angle/delay estimation are evaluated. We found that PN and PAN affect both angle and delay estimation, whereas CFO and MC have a more significant effect on angle estimation. We also observed that with perfect knowledge of the HWIs, the bound is close to the bound of the MM, but will saturate at a certain level in the high SNR regime due to the PAN. In conclusion, dedicated pilot signal design, HWIs estimation and mitigation algorithms are needed for accurate localization in 6G systems.

## ACKNOWLEDGMENT

This work was supported, in part, by the European Commission through the H2020 project Hexa-X (Grant Agreement

no. 101015956) and by the MSCA-IF grant 888913 (OTFS-RADCOM).

## APPENDIX A

The pseudo-true parameters can be calculated as

$$\boldsymbol{\theta}_0 = \arg \min_{\boldsymbol{\theta}} D_{\text{KL}}(f_{\text{TM}}(\mathbf{y}|\bar{\boldsymbol{\theta}}) \| f_{\text{MM}}(\mathbf{y}, \boldsymbol{\theta})).$$

After some manipulation, we find that

$$\begin{aligned} \boldsymbol{\theta}_0 &= \arg \min_{\boldsymbol{\theta}} \int f_{\text{TM}}(\mathbf{y}|\bar{\boldsymbol{\theta}}) \|\mathbf{y} - \boldsymbol{\mu}(\boldsymbol{\theta})\|^2 d\mathbf{y} \\ &= \arg \min_{\boldsymbol{\theta}} \sum_{g,k} \int f_{\text{TM}}(y_{g,k}|\bar{\boldsymbol{\theta}}) |y_{g,k} - \mu_{g,k}(\boldsymbol{\theta})|^2 d y_{g,k}. \end{aligned}$$

For each received symbol at the  $g$ th transmission and  $k$ th subcarrier,  $y_{g,k} \sim \mathcal{CN}(\bar{\mu}_{g,t}(\bar{\boldsymbol{\theta}}), \sigma_n^2)$ , by ignoring the indices  $g$  and  $k$  we can have

$$\begin{aligned} \int f_{\text{TM}}(y|\bar{\boldsymbol{\theta}}) |y - \mu(\boldsymbol{\theta})|^2 dy &= \int f_{\text{TM}}(y|\bar{\boldsymbol{\theta}}) |y - \bar{\mu}(\bar{\boldsymbol{\theta}})|^2 dy \\ &+ \int f_{\text{TM}}(y|\bar{\boldsymbol{\theta}}) |\bar{\mu}(\bar{\boldsymbol{\theta}}) - \mu(\boldsymbol{\theta})|^2 dy \\ &+ \int f_{\text{TM}}(y|\bar{\boldsymbol{\theta}}) |(y - \bar{\mu}(\bar{\boldsymbol{\theta}}))(\bar{\mu}(\bar{\boldsymbol{\theta}}) - \mu(\boldsymbol{\theta}))| dy \\ &= \sigma_n^2 + |\bar{\mu}(\bar{\boldsymbol{\theta}}) - \mu(\boldsymbol{\theta})|^2 + 0, \end{aligned}$$

from which (23) follows immediately.

## APPENDIX B

To obtain matrices  $\mathbf{A}$  and  $\mathbf{B}$ , we need to calculate the derivative of the noise-free version of the MM  $\boldsymbol{\mu}(\boldsymbol{\theta})$  with respect to the channel parameters inside the vector  $\boldsymbol{\theta}$ .

### A. First-order Derivatives

For the first-order derivative parts of the matrix  $\mathbf{A}$ , note that  $\alpha$  is dependent of  $\rho$  and  $\xi$ ,  $\mathbf{a}$  is dependent of AOA  $\vartheta$ ,  $\mathbf{D}$  is dependent of delay  $\tau$ . We can write  $\frac{\partial \mu_{g,k}}{\partial \vartheta} = \mathbf{w}_g^\top \alpha \tilde{\mathbf{C}} \dot{\mathbf{a}}_\vartheta D_k$ ,  $\frac{\partial \mu_{g,k}}{\partial \tau} = \mathbf{w}_g^\top \alpha \tilde{\mathbf{C}} \mathbf{a} \dot{D}_{k,\tau}$ ,  $\frac{\partial \mu_{g,k}}{\partial \rho} = \mathbf{w}_g^\top \dot{\alpha}_\rho \tilde{\mathbf{C}} \mathbf{a} D_k$ ,  $\frac{\partial \mu_{g,k}}{\partial \xi} = \mathbf{w}_g^\top \dot{\alpha}_\xi \tilde{\mathbf{C}} \mathbf{a} D_k$ . where  $\dot{D}_{k,\tau} = -j2\pi k \Delta_f D_k$ ,  $\dot{\alpha}_\rho = e^{-j\xi}$ ,  $\dot{\alpha}_\xi = -j\alpha$  and  $\dot{\mathbf{a}}_\vartheta = [0, j\pi \cos(\vartheta), \dots, j(N-1)\pi \cos(\vartheta)]^\top \odot \mathbf{a}$ .

### B. Second-order Derivatives

The second-order derivative parts of the matrix  $\mathbf{B}$  in equation (25) can be obtained based on the dependence of the channel components  $(\alpha, \mathbf{a}, D)$  and unknowns  $(\vartheta, \tau, \rho, \xi)$  with several examples as  $\frac{\partial^2 \mu_{g,k}}{\partial \vartheta \partial \vartheta} = \mathbf{w}_g^\top \alpha \tilde{\mathbf{C}} \ddot{\mathbf{a}}_\vartheta D_k$ ,  $\frac{\partial^2 \mu_{g,k}}{\partial \theta \partial \tau} = \mathbf{w}_g^\top \alpha \tilde{\mathbf{C}} \dot{\mathbf{a}}_\theta \dot{D}_{k,\tau}$ ,  $\frac{\partial^2 \mu_{g,k}}{\partial \tau \partial \tau} = \mathbf{w}_g^\top \alpha \tilde{\mathbf{C}} \mathbf{a} \ddot{D}_{k,\tau}$ ,  $\frac{\partial^2 \mu_{g,k}}{\partial \rho \partial \rho} = \mathbf{w}_g^\top \dot{\alpha}_\rho \tilde{\mathbf{C}} \mathbf{a} D_k$ , and  $\frac{\partial^2 \mu_{g,k}}{\partial \rho \partial \xi} = \mathbf{w}_g^\top \dot{\alpha}_{\rho,\xi} \tilde{\mathbf{C}} \mathbf{a} D_k$ . where  $\ddot{\mathbf{a}}_\vartheta = [0, j\pi \cos(\theta), \dots, j(N-1)\pi \cos(\theta)]^\top \odot \mathbf{a}$ ,  $\ddot{D}_{k,\tau} = -j2\pi k \Delta_f \dot{D}_k$ ,  $\dot{\alpha}_\rho = 0$ ,  $\dot{\alpha}_\xi = -\alpha$ , and  $\dot{\alpha}_{\rho,\xi} = -je^{-j\xi}$ .

## REFERENCES

- [1] R. Di Taranto *et al.*, “Location-aware communications for 5G networks: How location information can improve scalability, latency, and robustness of 5G,” *IEEE Signal Process. Mag.*, vol. 31, no. 6, pp. 102–112, Oct. 2014.
- [2] G. Kwon *et al.*, “Joint communication and localization in millimeter wave networks,” *IEEE J. Sel. Topics Signal Process.*, Sep. 2021.
- [3] Z. Xiao *et al.*, “An overview on integrated localization and communication towards 6G,” *Sci. China Inf. Sciences*, vol. 65, no. 3, pp. 1–46, Mar. 2022.
- [4] H. Chen *et al.*, “A tutorial on terahertz-band localization for 6G communication systems,” *arXiv preprint arXiv:2110.08581*, Oct. 2021.
- [5] O. Kolawole *et al.*, “Impact of hardware impairments on mmwave MIMO systems with hybrid precoding,” in *IEEE Wireless Commun. Netw. Conf.*, Apr. 2018.
- [6] H. Shen *et al.*, “Beamforming optimization for IRS-aided communications with transceiver hardware impairments,” *IEEE Trans. Commun.*, vol. 69, no. 2, pp. 1214–1227, Oct. 2020.
- [7] Y. Wu *et al.*, “Efficient channel estimation for mmwave MIMO with transceiver hardware impairments,” *IEEE Trans. Veh. Technol.*, vol. 68, no. 10, pp. 9883–9895, Aug. 2019.
- [8] N. Ginige *et al.*, “Untrained DNN for channel estimation of RIS-assisted multi-user OFDM system with hardware impairments,” in *IEEE 32nd Annu. Int. Symp. Pers. Indoor Mobile Radio Commun.*, Sep. 2021, pp. 561–566.
- [9] H. C. Yildirim *et al.*, “Impact of phase noise on mutual interference of FMCW and PMCW automotive radars,” in *16th Eur. Radar Conf.* IEEE, Oct. 2019, pp. 181–184.
- [10] M. Gerstmair *et al.*, “On the safe road toward autonomous driving: Phase noise monitoring in radar sensors for functional safety compliance,” *IEEE Signal Process. Mag.*, vol. 36, no. 5, pp. 60–70, Sep. 2019.
- [11] K. Siddiq *et al.*, “Phase noise in FMCW radar systems,” *IEEE Trans. Aerosp. Electron. Syst.*, vol. 55, no. 1, pp. 70–81, Feb 2019.
- [12] Z. Ye *et al.*, “DOA estimation for uniform linear array with mutual coupling,” *IEEE Trans. Aerosp. Electron. Syst.*, vol. 45, no. 1, pp. 280–288, Mar. 2009.
- [13] F. Ghasemianj *et al.*, “Localization error bounds for 5G mmWave systems under I/Q imbalance,” *IEEE Trans. Veh. Technol.*, vol. 69, no. 7, pp. 7971–7975, Apr. 2020.
- [14] F. Bozorgi *et al.*, “RF front-end challenges for joint communication and radar sensing,” in *1st IEEE Int. Online Symp. Joint Commun. Sens.*, Feb. 2021.
- [15] F. Ghasemianj *et al.*, “Localization error bounds for 5G mmWave systems under hardware impairments,” in *IEEE 32nd Annu. Int. Symp. Pers. Indoor Mobile Radio Commun.*, Sep. 2021, pp. 1228–1233.
- [16] C. D. Richmond *et al.*, “Parameter bounds on estimation accuracy under model misspecification,” *IEEE Trans. Signal Process.*, vol. 63, no. 9, pp. 2263–2278, Mar. 2015.
- [17] F. Roemer, “Misspecified Cramér-Rao bound for delay estimation with a mismatched waveform: A case study,” in *IEEE Int. Conf. Acoust., Speech Signal Process.*, May. 2020, pp. 5994–5998.
- [18] S. Fortunati *et al.*, “Performance bounds for parameter estimation under misspecified models: Fundamental findings and applications,” *IEEE Signal Process. Mag.*, vol. 34, no. 6, pp. 142–157, Nov. 2017.
- [19] T. Schenk, *RF imperfections in high-rate wireless systems: Impact and digital compensation*. Springer Science & Business Media, 2008.
- [20] A. Mohammadian *et al.*, “RF impairments in wireless transceivers: Phase noise, CFO, and IQ imbalance—A survey,” *IEEE Access*, vol. 9, pp. 111718–111791, Aug. 2021.
- [21] N. Hajiabdolrahim *et al.*, “An extended Kalman filter framework for joint phase noise, CFO and sampling time error estimation,” in *31st Annu. Int. Symp. Pers. Indoor Mobile Radio Commun.* IEEE, 2020.
- [22] D. L. Lin *et al.*, “Joint estimation of channel response, frequency offset, and phase noise in OFDM,” *IEEE Trans. Signal Process.*, vol. 54, no. 9, pp. 3542–3554, Aug. 2006.
- [23] O. H. Salim *et al.*, “Channel, phase noise, and frequency offset in OFDM systems: Joint estimation, data detection, and hybrid cramér-rao lower bound,” *IEEE Trans. Commun.*, vol. 62, no. 9, pp. 3311–3325, Jul. 2014.
- [24] M. Chung *et al.*, “Phase-noise compensation for OFDM systems exploiting coherence bandwidth: Modeling, algorithms, and analysis,” *IEEE Trans. Wireless Commun.*, Oct. 2021.
- [25] T. Roman *et al.*, “Blind frequency synchronization in OFDM via diagonality criterion,” *IEEE Trans. Signal Process.*, vol. 54, no. 8, pp. 3125–3135, Jul. 2006.
- [26] J. Nocedal *et al.*, *Numerical optimization*. Springer Science & Business Media, 2006.
- [27] A. Elzanaty *et al.*, “Reconfigurable intelligent surfaces for localization: Position and orientation error bounds,” *IEEE Trans. Signal Process.*, vol. 69, pp. 5386–5402, Aug. 2021.